ROBOTICS

Launching by cavitation

Dalei Wang[1]†, Zixiao Liu[2]†, Hongping Zhao[1]†, Huanqi Qin[1]†, Gongxun Bai[3], Chi Chen[2], Pengju Shi[2], Yingjie Du[2], Yusen Zhao[2], Wei Liu[1]*, Dan Wang[4]*, Guoquan Zhou[1]*, Ximin He[2]*, Chaoqing Dai[1]*

Cavitation, characterized by formation of vapor bubbles in a low-pressure or high-temperature region of a liquid, is often destructive, but it can be harnessed for actuators and robots. We exploit cavitation to accumulate substantial energy in superheated liquids by suppressing its immediate release until reaching a stability limit. The energetic, unstable bubbles collapse violently, producing a burst of high power and force that initiates motion. Notably, a millimeter-scale device launched by cavitation can jump to a height of 1.5 meters—reaching a 12 meters per second (m/s) peak velocity, a 7.14×10^4 m/s^2 acceleration, and a 0.64% energy efficiency—and can also swim on water at 12 centimeters per second. Cavitation-based launching works with a broad range of device materials, liquid media, stimuli, and operational environments.

Launching propels a system from a state of rest or low speed into rapid motion by storing substantial energy and swiftly releasing it, generating a potent burst of power and force that initiates motions, such as jumping, sprinting, swimming, and flying. Inspired by biological muscles' elastic energy ($U = \int_V 0.5k\varepsilon^2 dV$) is widely harnessed for artificial launching. Strategies to improve launch performance typically focus on increasing elastic energy storage by optimizing material stiffness k and deformability ε_{max}, or by enhancing the energy release rate dU/dt through mechanical instabilities. For example, snap-through buckling enables considerable energy storage by creating a high energy barrier through tailored mechanical properties and geometric designs (*1*), while its intrinsic instability promotes rapid energy release (*2*, *3*). Additionally, antagonistic structures with self-latching mechanisms, as observed in insect flight, can effectively amplify power output. In these systems, the contraction of an agonist muscle pre-stretches its antagonist, and the sudden relaxation of these muscles explosively releases the stored energy. This mechanism is exemplified by an engineered jumper that combines the compression of a structural frame (agonist; energy density $\Gamma = 1922$ J/kg) with the tension of multiple elastic linkages (antagonist; $\Gamma = 7000$ J/kg), enabling a 0.3-m device to achieve a jump height of ~32 m (*4*). However, solid structures generally exhibit limited energy storage capacity and slow deformation rates, inherently constraining the performance of elastic energy–based launchers.

To overcome these limitations, phase-transition processes capable of delivering higher energy and faster dynamics have increasingly been used. For instance, by loading high-energy propellants and explosives with high Γ (e.g., butane, $\Gamma = 49.5$ MJ/kg) into jumpers and harnessing their rapid, substantial volumetric expansion during combustion (*5*–*7*), insect-scale jumpers can reach a height of 59 cm (*8*). Similarly, inducing water boiling (Γ = 2260 kJ/kg) in hydrogels via photothermal stimulation (*9*, *10*) can trigger bubble expansion that exceeds the hydrogel's fracture strain (*10*). This sudden structural failure rapidly releases energy and amplifies launch power. However, devices based on the fracture-driven mechanism are single-use, and their performance remains suboptimal: The less intense dynamics of boiling restrict both the amount and rate of energy release.

Cavitation is a highly dynamic and energetic liquid-vapor transition process in which vapor bubbles nucleate, explosively expand, and violently collapse in response to local pressure drops or elevated temperatures. Unlike boiling, which releases less energy over a longer duration (several to tens of milliseconds), cavitation can accumulate greater energy in a superheated state, and its highly energetic, unstable nature enables an ultrafast energy release on a microsecond timescale (*11*), producing ultrahigh-pressure output. Cavitation is typically regarded as destructive in industrial contexts, where it can mechanically erode hard alloys within a microsecond by generating pressures of several hundred megapascals (*12*). However, if its immense output and ultrafast dynamics can be effectively harnessed, cavitation may potentially enhance the performance of actuators, robots, and other engineered devices. Nature has evolved ingenious ways to exploit cavitation: fern sporangia utilize cavitation within dehydrated annulus cells to trigger rapid bending, launching spores at high velocities of ~10 m/s (*13*, *14*). Similarly, mantis shrimps swiftly snap their appendages to induce hydrodynamic cavitation, delivering mechanical impact–cavitation shockwave dual strikes with large forces of ~1500 N on their prey (*15*).

We use cavitation as a launching mechanism for rapid motion. The rapid transmission of substantial energy during cavitation produces a burst of power and acceleration, imparting high kinetic energy to the launched objects. This mechanism can be triggered by various stimuli to launch devices made from different materials across a wide range of operational environments.

Jumpers launched by photothermal cavitation

Although cavitation can be induced by various stimuli, including lasers, electrical sparks, and ultrasound, we found that photothermal cavitation delivers the best motion performance while enabling remote activation. Therefore, we selected photothermal cavitation–launched jumpers to analyze the launching mechanism. Various photothermal materials can be used to construct the jumpers, but they generally need to meet three key requirements: (i) high photothermal efficiency for rapid heat generation, (ii) high mechanical robustness and thermal stability to withstand extreme pressure and temperature conditions during cavitation, and (iii) adjustable density for deployment in diverse operational environments. A titanium dioxide–polypyrrole–titanium carbide (TiO_2-PPy-TiC) composite was used [fig. S4A and supplementary materials (SM) sections M1 and M2]. TiC exhibits high near-infrared (NIR) absorbance (fig. S4K), enhancing the system's photothermal efficiency to 84.47% (SM section S1 and fig. S4, I and J) (*16*, *17*)], which enables rapid heating of the surrounding liquid to the superheated state and triggers cavitation. TiO_2 ensures thermal stability above 300°C (figs. S4L and S5), while the branched, interconnected PPy network binds TiC and TiO_2 (fig. S4, B to H), effectively resisting large impact forces. By adjusting TiO_2 concentration to tune the material density, the jumper can either float on or submerge in various liquids. The final dimensions of TiO_2-PPy-TiC-based jumpers are 1 mm by 1 mm by 0.2 mm, with a mass of 0.778 mg.

When deployed on a transparent solid surface moistened with a few water droplets and irradiated from below with an 808-nm near-infrared laser at 0.357 kW/cm^2, the millimeter-scale TiO_2-PPy-TiC jumper achieved a height of 1.5 m (Fig. 1A and movie S1), with a takeoff velocity >12 m/s (Fig. 1B), and an acceleration exceeding 7.14×10^4 m/s^2 (SM section S3). This performance stems from the high impact pressure (280 kPa; SM section S3) delivered by cavitating jets, which accelerate the jumper from rest to 12 m/s within just 0.168 ms [Fig. 1E, (III) to (V)]. The takeoff velocity and acceleration time surpass those observed in the cavitation-assisted spore dispersal of ferns (10 m/s; 1 s) (*14*).

[1]National Key Laboratory for Development and Utilization of Forest Food Resources, Zhejiang A&F University, Hangzhou, China. [2]Department of Materials Science and Engineering, University of California, Los Angeles, Los Angeles, CA, USA. [3]College of Optical and Electronic Technology, China Jiliang University, Hangzhou, China. [4]School of Chemistry and Chemical Engineering, Anhui University of Technology, Ma'anshan, Anhui, China. ***Corresponding author. Email: liuwei@zafu.edu.cn (W.L.); wangdan@ahut.edu.cn (D.W.); 19920006@zafu.edu.cn (G.Z.); ximinhe@ucla.edu (X.H.); dcq424@zafu.edu.cn (C.D.)** †These authors contributed equally to this work.

Launching mechanism

Upon laser irradiation, the local temperature beneath the jumper rapidly exceeds the liquid's boiling point T_b, driving the water into a metastable state. Photothermal energy deposition intensifies molecular motion, raising internal pressure P_{in}. When the temperature reaches the liquid's superheat limit T_t, a cavity nucleates and destabilizes, explosively expanding against the surrounding liquid [Fig. 1E, (I) to (III)] and storing potential energy. This volumetric expansion elevates the jumper [Fig. 1E, (II)] over a duration of 0.624 ms until the bubble attains its maximum radius [Fig. 1E, (III)]. During the bubble growth, its internal pressure P_{in} decreases until it falls below the outside pressure P_{out}, triggering the rapid collapse over the subsequent 0.144 ms [Fig. 1E, (III) and (IV)]. As the bubble contracts, surrounding liquid rushes into the space previously occupied by the bubble at speeds up to 57.1 m/s (fig. S6). The collision of these high-speed flows generates a powerful upward jet [Fig. 1E, (IV) and (V)] that strikes the jumper with a pressure of 280 kPa (SM section S3). The complete cavitation-induced launch process is documented in movie S2. Our TiO_2-PPy-TiC material demonstrates excellent mechanical durability and thermal stability under extreme pressure and thermal conditions during cavitation, enabling over 500 repeated launch cycles without structural disintegration (Fig. 1D). Our cavitation-based launching strategy is applicable to objects made from various materials. For instance, thin platelets of pure candle soot (CS), carbon dots (CD), graphite (GR), or black metals can also be launched with decent performance (Fig. 1C). The photothermal agent TiC can be replaced with alternatives x, such as CS, CD, or GR, to fabricate TiO_2-PPy-x photothermal composites.

We introduced an analytical model to quantitatively analyze the pressure burst, energy conversion, and bubble evolution during cavitation. To clearly observe bubble morphology and jet formation, we temporarily removed the jumper (Fig. 2A and movies S3 and S4). The observed cavitation timescales (Fig. 2B) differ slightly from those in Fig. 1E because the absence of fluid-structure interaction alters the bubble dynamics. The experimentally measured maximum bubble radius $R_{max} \approx 750$ μm was used as the initial condition for the model. The dynamics of the liquid and gas phases were governed by the Navier-Stokes and continuity equations, with the gas described by the Noble-Abel equation of states and the compressible liquid by the Tait equation. Bubble radius evolution $R(t)$ during the collapse was modeled using the Gilmore model (*18*),

$$\left(1-\frac{\dot{R}}{C}\right)R\ddot{R}+\frac{3}{2}\left(1-\frac{\dot{R}}{3C}\right)\dot{R}^2=\left(1+\frac{\dot{R}}{C}\right)H+\left(1-\frac{\dot{R}}{C}\right)\frac{R}{C}\dot{H} \quad (1)$$

where H and C denote the specific enthalpy difference and speed of sound, respectively. Detailed model derivations and variable expressions are provided in SM section S4 and (*18*). Figure 2C shows the simulated variations in bubble radius $R(t)$ and pressure during bubble contraction and collapse. The bubble contracts from R_{max} of 750 μm to a minimum radius R_{min} of 88.4 μm within 72 μs. During contraction, stored potential energy $E_p = \int (P_{out} - P_{in})dV$ is converted into kinetic energy $E_k = 0.5\rho V(dR/dt)^2$ (Fig. 2D). Both contraction rate dR/dt (fig. S6) and the kinetic energy E_k increase as $R(t)$ decreases, with $|dR/dt|$ peaking at 57.1 m/s just before the bubble reaches R_{min}. The subsequent bubble collapse generates a jet with a peak pressure of 10.2 MPa (Fig. 2C), which decays to an impact pressure of 280 kPa on the jumper, as determined experimentally (SM section S3). This decay is attributed to liquid drag and energy losses during momentum exchange at impact. During the bubble collapse, the kinetic energy E_k drops from its peak to zero almost instantaneously (within 8.4 μs), converting into a burst of potential energy E_p (Fig. 2D). Finite volume simulations using the volume of fluid method in OpenFOAM validated the bubble's morphological changes and jet formation [movie S4 and Fig. 2E, (I) to (IV)].

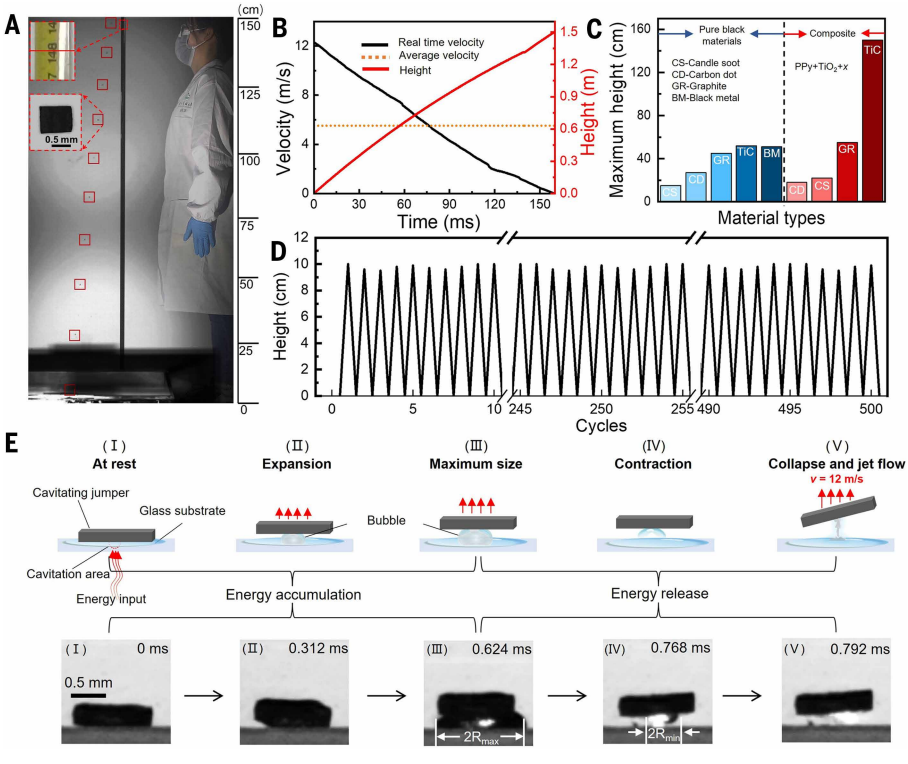

Fig. 1. Jumpers launched by photothermal cavitation. (**A**) Superimposed images depict a jump launched by photothermal cavitation reaching a peak height of 1.5 m (movie S1). Insets provide a magnified view of the ruler scale used for height measurement and a close-up of the TiO_2-PPy-TiC–based photothermal jumper. (**B**) Real-time measurements of velocity and displacement, along with average velocity of jumping. The takeoff velocity can reach 12 m/s. (**C**) Maximum jumping heights of cavitation-launched jumpers irradiated by a laser with the same intensity (0.357 kW/cm^2). Blue bars represent devices constructed from various pure black materials, whereas red bars indicate jumpers fabricated using TiO_2-PPy with different photothermal agents (x). (**D**) Durability test results for the TiO_2-PPy-TiC jumper demonstrate no structural disintegration over 500 launch cycles (experimental setup shown in fig. S1). (**E**) Schematic of the launching mechanism based on cavitation, accompanied by corresponding high-speed photography (movie S2).

Influence of liquid properties and environmental factors on jumping performance

We launched our TiO_2-PPy-TiC jumpers in various liquids (SM section M6) to study how liquid properties—such as compressibility, available nucleation sites, viscosity, and surface tension—affect launch performance (Fig. 2F). In more compressible liquids such as ethanol, jumpers perform less efficiently than in water primarily because water's lower compressibility resists volume change during bubble collapse, enabling greater energy accumulation and a more violent release. Additionally, preexisting nucleation sites influence bubble dynamics: In saline solutions, ion-dipole interactions between salt ions and water molecules form hydration shells, reducing free water concentration and air solubility, which may introduce noncondensable gas bubbles. These bubbles serve as nucleation sites for cavities, promoting premature cavitation (*19*). Besides, the noncondensable gas also acts as a cushion that softens bubble collapse (*20*, *21*),

which further diminishes jumping performance. We also increased liquid viscosity by dissolving polyvinyl alcohol (PVA) in water. The dynamic viscosities of 2.5 weight % (wt %) and 4.5 wt % PVA solutions were measured to be 0.05 and 0.08 Pa·s, respectively, which are much higher than that of water (~0.001 Pa·s). Jumpers in these PVA solutions exhibited reduced performance compared with those in pure water. Our numerical simulations indicated that cavitation pressure remains similar across viscosities, suggesting that the compromised performance primarily stems from increased liquid drag during upward jumping rather than cavitation pressure output. Lastly, jumpers were tested in 0.1 and 0.3 wt % soap water, which exhibited equilibrium surface tensions of 0.036 and 0.027 kg/s^2, respectively. The ultrafast nature of cavitation limits surfactant adsorption at the bubble-liquid interface, so dynamic surface tension needs to be considered (fig. S7). However, our analytical model shows that Laplace pressure from surface effects is several orders of magnitude lower than the bubble's internal pressure (fig. S8), which explains the negligible difference in jumping performance between water and soap solutions.

Liquid depth and laser intensity also influence launch and motion performance. Greater liquid depth requires the jumper to expend more energy overcoming liquid drag, thereby reducing its jumping height (fig. S9). Additionally, a minimum laser intensity I_0 (>0.087 kW/cm^2) is necessary to deposit enough energy to shift the system from a metastable to an unstable state and initiate cavitation (Fig. 2G). At I_0 = 0.357 kW/cm^2, water reaches its superheat limit (303.1°C; fig. S10), yielding optimal jumper performance. However, further increases in I_0 may lead to excessively intense bubble expansion, causing premature collapse before the bubble reaches its theoretical maximum size, which reduces the pressure

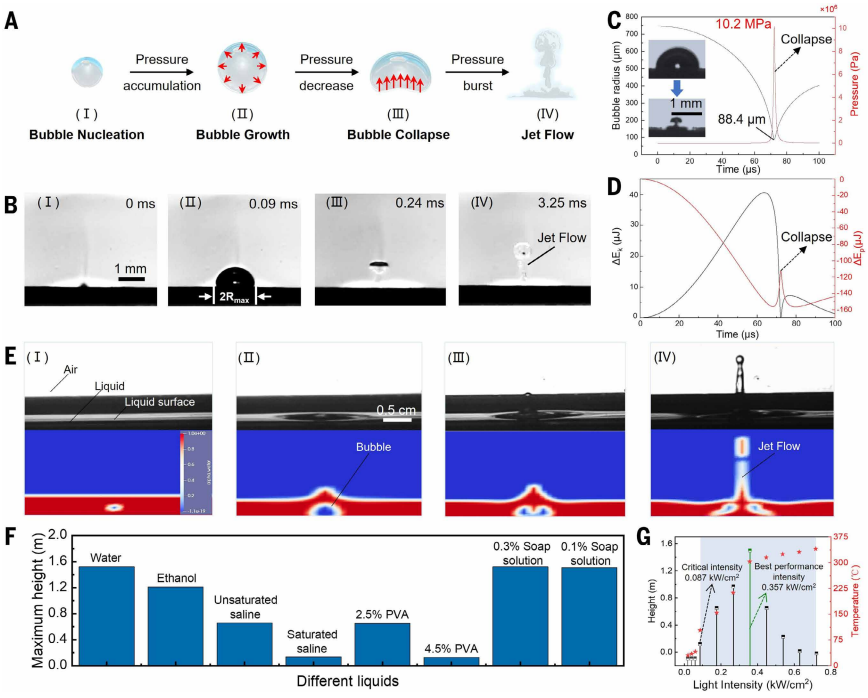

Fig. 2. Mechanism of cavitation-triggered launching and influence factors. (**A**) Schematic diagram and (**B**) high-speed photography (movie S3) capturing the cavitation process in detail, including bubble morphology evolution and jet flow generation. (**C**) Simulation results showing the evolution of bubble radius $R(t)$ and internal pressure $P_{in}(t)$ during bubble contraction and collapse. Insets display the experimental observations of bubble morphologies at maximum radius R_{max} and the jet formation upon collapse. (**D**) Simulated energy conversion between potential energy $E_p = \int (P_{out} - P_{in})dV$ and kinetic energy $E_k = 0.5\rho V(dR/dt)^2$ during bubble cavitation. (**E**) High-speed photography (movie S4), illustrating jet flow ejection from the water surface, alongside finite volume simulation results. (**F**) Jumping performance when launched from different liquids. (**G**) Jumping performance under varying light intensities.

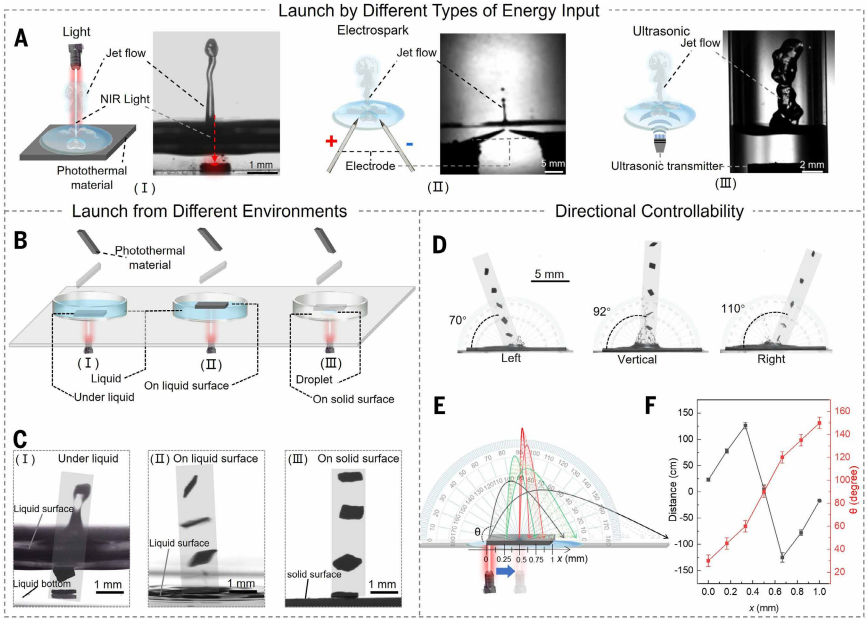

Fig. 3. Generality and controllability of cavitation-triggered launching. (**A**) Schematic and high-speed photography (movie S5) illustrate cavitation jets induced by different stimuli: (I) laser, (II) electrical spark, and (III) ultrasound. (**B**) Schematic diagram and (**C**) high-speed photography (movie S6) show the launches from diverse environments: (I) under liquid, (II) on liquid surfaces, and (III) on wet solid surfaces. (**D**) High-speed photography (movie S7) demonstrates controlled directional launches—leftward, vertical, and rightward—achieved by targeting laser irradiation on the right, center, and left portions of the jumper, respectively. (**E**) Schematic representation of the strategy for precisely controlling launch angle and horizontal launch distance. (**F**) Correlation between horizontal launch distance, launch angle, and laser irradiation position.

output and performance. We also tested jumpers of other shapes, including cones with different diameter-to-height ratios and hemispheres. Their uneven mass distribution increases airborne tumbling compared to flat platelets, dissipating more kinetic energy and reducing jumping height (fig. S11).

Generality and controllability

In addition to photothermal stimulation [Fig. 3A, (I)], cavitation can also be activated by electrical sparks and ultrasound (movie S5). Electrical sparks ionize water molecules, forming plasma that rapidly expands to generate spark-induced cavitation. This cavitation produces a jet flow [Fig. 3A, (II)], which can launch a photothermally nonresponsive polytetrafluoroethylene (PTFE) platelet to a height of 0.93 m (fig. S12F). Spark-induced cavitation does not rely on the material's photothermal properties or substrate transparency to allow light to pass through, making it a viable alternative to photothermal cavitation. Moreover, compact sparking electrodes can be easily embedded in robots as onboard power sources. Ultrasound transmits high-intensity compression and rarefaction waves into the liquid, reducing local pressure and forming acoustic cavitation bubbles. Notably, ultrasound creates a large low-pressure region that can

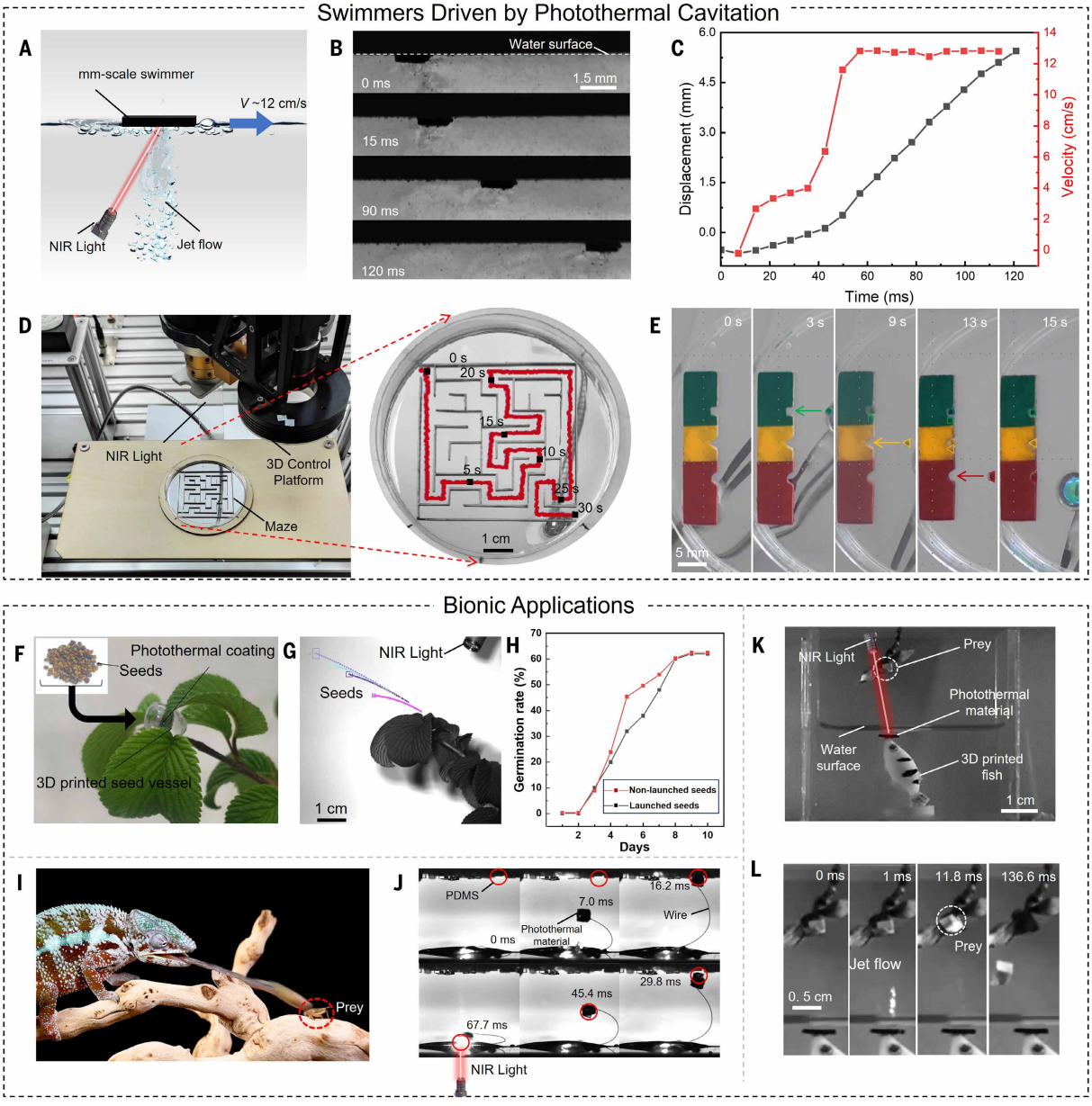

Fig. 4. Swimmers propelled by cavitating jets and bionic applications of cavitation-triggered launching. (**A**) Schematic of a swimmer driven by photothermal cavitation, achieving a swimming speed of ~12 cm/s. (**B**) Photographic sequence capturing the swimming within 120 ms. (**C**) Swimming speed and distance versus time. (**D**) A swimmer navigated a complex maze, closely following the laser movement (movie S8). The inset displays the maze layout, with the swimmer's trajectory indicated by red lines and black squares marking its positions at different times (0 to 30 s). (**E**) Swimmers of various shapes (square, triangular, and trapezoidal shapes) being directed toward and precisely fitting into corresponding notches (movie S8). (**F**) Photograph of the cavitation-assisted seeding system and (**G**) trajectories of launched seeds (movie S9). (**H**) Comparable germination rates between seeds launched by photothermal cavitation and untreated seeds, demonstrating the potential for launching delicate objects by cavitation. (**I**) Chameleons ballistically project their tongues to swiftly and precisely capture prey, which inspires (**J**) the design of an object retrieval system (movie S9). PDMS, polydimethylsiloxane. (**K**) Schematic of an archerfish-inspired liquid jetting system. (**L**) Sequential snapshots from movie S9, depicting the jetting process over 136.6 ms.

simultaneously induce multiple bubbles (fig. S12D). Therefore, acoustic cavitation [Fig. 3A, (III)] may have the potential to launch large-scale objects (fig. S12E) or simultaneously launch multiple objects.

The versatility of our launching strategy is further demonstrated by its adaptability to various environments. Our photothermal jumpers can be deployed under liquids, on liquid surfaces, and on solid surfaces (Fig. 3, B and C, and movie S6), accommodating diverse application scenarios. The jumpers perform best on wet solid surfaces, whereas their performance diminishes as they are submerged in liquids (fig. S13). Because initiating single-bubble cavitation requires only a small amount of liquid, even residual solvent within the jumper material is sufficient to induce cavitation (fig. S13D), thereby minimizing reliance on external liquid environments. However, because cavitation occurs within the launcher without the buffering effect of surrounding liquid, repeated launches may compromise structural integrity.

The substantial force generated by cavitation may raise concerns about precise control over launch direction and trajectory. By adjusting the position of laser irradiation on the jumper (Fig. 3, D and E), the point of force application can be altered, enabling launching over a wide three-dimensional (3D) range (Fig. 3F). For instance, irradiating the right portion of the jumper produces cavitation that generates a counterclockwise rotational moment, elevating its right end and launching the jumper leftward (Fig. 3D and movie S7). Adjusting the launch angle yields different horizontal distances, with a maximum of 1.26 m achieved at angles of 155° and 25° (Fig. 3F).

Swimmers propelled by photothermal cavitation

Cavitation is capable of launching a range of motions beyond simple jumping. By controlling fluid-structure interactions during cavitation near a solid, a millimeter-scale swimmer driven by photothermal cavitation can be engineered. A TiO_2-PPy-TiC platelet was positioned on the water surface. When irradiated from below at an oblique angle and guided by a laser moving at up to 12 cm/s (Fig. 4A), the swimmer accelerates to match the laser's speed and closely follows its trajectory (Fig. 4B and movie S8). A 1.5-mm-long cavitation-driven swimmer can achieve a high swimming speed of ~12 cm/s (Fig. 4C). The moving, obliquely angled laser creates an asymmetric temperature field that initiates a downward cavitating jet at an angle. This jet rebounds toward the water surface and forms an asymmetric loop flow that not only propels the swimmer but also confines it within the irradiated region. Surface tension at the water-air interface prevents the swimmer from being launched into the air. The swimming motion is highly controllable, enabling navigation through complex, confined environments such as mazes (Fig. 4D and movie S8) and microfluidic channels. Additionally, swimmers of various shapes can be guided to fit seamlessly into corresponding notches (Fig. 4E and movie S8), highlighting potential applications in precision assembly, circuit repair, micromanipulation, and beyond (*22*). The millimeter-scale TiO_2-PPy-TiC platelet can also be deployed on the water's bottom and swim at 3 cm/s (fig. S14 and movie S8).

Bioinspiration and potential applications

Biological organisms have evolved various launching mechanisms for rapid movement and powerful actions essential for hunting, reproduction, and other physiological functions. For example, ferns exploit hydrodynamic cavitation within their sporangia to forcefully eject spores for wide dispersal. Inspired by this, we investigated whether photothermal cavitation could similarly propel delicate objects like seeds without compromising their structural integrity or functionality, despite the high local pressures and temperatures. *Oxalis* seeds (1 to 2 mm in diameter) were placed in a custom-built, water-filled container with its bottom coated in our TiO_2-PPy-TiC material (Fig. 4F). Upon irradiation, photothermal cavitation successfully launched the seeds (Fig. 4G and movie S9) to distances >0.7 m (fig. S15). The germination rates of the cavitation-launched seeds were comparable to those of untreated seeds (Fig. 4H). This model scenario thus demonstrates the potential of photothermal cavitation for safely transporting fragile objects—such as microcircuitry, sensors, and signal transmitters—into confined and inaccessible environments. To retrieve objects from such environments, we developed a microscale cargo retrieval device inspired by the chameleon's ballistic tongue (Fig. 4I and fig. S16A). A sticky TiO_2-PPy-TiC gripper was attached to a fixed substrate via a flexible wire. Upon irradiation, the gripper is precisely launched toward the target position to retrieve cargo (Fig. 4J, fig. S17, and movie S9).

Inspired by the archerfish, we also developed a cavitation-powered liquid jetting system by affixing a TiO_2-PPy-TiC material to an underwater substrate (a 3D-printed archerfish in Fig. 4K). Upon cavitation, a high-speed jet with an initial velocity of ~1.8 m/s (fig. S16D) was generated, reaching a maximum height of ~10 cm (fig. S18 and movie S9). The rapid energy transmission of cavitation enables continuous jetting, with intervals of less than 10 ms between successive jets. This high-speed, high-pressure (Fig. 2C) liquid jet has the potential to penetrate biological tissues and inject drugs, providing a promising alternative to needle-based drug injections (*23*).

In conclusion, our study demonstrates that cavitation can serve as an efficient launching mechanism. The rapid transmission of substantial energy during cavitation produces a burst of power and acceleration, imparting high kinetic energy to the launched objects. The jumpers and swimmers launched by cavitation exhibit decent performance. With compatibility across a wide range of device materials, liquid media, external stimuli, and operational environments, our cavitation-based launching strategy can be tailored to meet the demands of different applications.

REFERENCES AND NOTES

1. J. Hu *et al.*, *Angew. Chem. Int. Ed.* **62**, e202218227 (2023).
2. Y. Kim, J. van den Berg, A. J. Crosby, *Nat. Mater.* **20**, 1695–1701 (2021).
3. H. Lee, C. Xia, N. X. Fang, *Soft Matter* **6**, 4342–4345 (2010).
4. E. W. Hawkes *et al.*, *Nature* **604**, 657–661 (2022).
5. M. Loepfe, C. M. Schumacher, U. B. Lustenberger, W. J. Stark, *Soft Robot.* **2**, 33–41 (2015).
6. W. A. Churaman, L. J. Currano, C. J. Morris, J. E. Rajkowski, S. Bergbreiter, *J. Microelectromech. Syst.* **21**, 198–205 (2012).
7. N. W. Bartlett *et al.*, *Science* **349**, 161–165 (2015).
8. C. A. Aubin *et al.*, *Science* **381**, 1212–1217 (2023).
9. M. Li, X. Wang, B. Dong, M. Sitti, *Nat. Commun.* **11**, 3988 (2020).
10. X. Wang *et al.*, *Nat. Mater.* **23**, 1428–1435 (2024).
11. V. P. Carey, *Liquid-Vapor Phase-Change Phenomena: An Introduction to the Thermophysics of Vaporization and Condensation Processes in Heat Transfer Equipment* (CRC Press, 2020).
12. M. Koch, thesis, Göttingen, Georg-August Universität (2020).
13. A. L. King, *Proc. Natl. Acad. Sci. U.S.A.* **30**, 155–161 (1944).
14. X. Noblin *et al.*, *Science* **335**, 1322–1322 (2012).
15. N. A. Alderete *et al.*, *Science* **387**, 659–666 (2025).
16. D. K. Roper, W. Ahn, M. Hoepfner, *J. Phys. Chem. C Nanomater. Interfaces* **111**, 3636–3641 (2007).
17. Y. Liu *et al.*, *Adv. Mater.* **25**, 1353–1359 (2013).
18. M. Koch *et al.*, *Comput. Fluids* **126**, 71–90 (2016).
19. Y. Huang, X. Qin, *Cryogenics* **146**, 104016 (2025).
20. T. Trummler, L. Freytag, S. J. Schmidt, N. A. Adams, in *Proceedings of the 10th International Symposium on Cavitation CAV* (ASME Press, 2018), pp. 656–659.
21. L. Tian *et al.*, *Int. Commun. Heat Mass Transf.* **145**, 106815 (2023).
22. Y. Sun *et al.*, *Angew. Chem. Int. Ed.* **59**, 1098–1102 (2020).
23. G. Arrick *et al.*, *Nature* **636**, 481–487 (2024).

ACKNOWLEDGMENTS

Funding: National Natural Science Foundation of China (grant no. 12261131495 and 12475008) (C.D.), National Natural Science Foundation of China (grant no. 12374281) (G.Z.), Scientific Research and Developed Fund of Zhejiang A&F University (grant no. 2021FR0009) (C.D.). **Author contributions:** Conceptualization: D.L.W., X.H., Z.L., W.L., C.D. Methodology: D.L.W., Z.L., X.H., H.Z., H.Q., G.B., W.L., D.W., G.Z., C.D. Investigation: D.L.W., Z.L., H.Q., H.Z., H.Q. Visualization: D.L.W., Z.L., H.Q., H.Z., H.Q. Funding acquisition: D.L.W., W.L., C.D. Project administration: X.H., Z.L., W.L., D.W., G.Z., C.D. Supervision: X.H., W.L., D.W., G.Z., C.D. Writing – original draft: Z.L., X.H., D.L.W., H.Z., W.L., D.W., CD. Writing – review & editing: Z.L., X.H., D.L.W., G.B., H.Z., C.C., P.S., Y.D., W.L., D.W., G.Z., C.D. **Competing interests:** The authors declare that they have no competing interests. **Data and materials availability:** All data are available in the main text or the supplementary materials.

SUPPLEMENTARY MATERIALS

science.org/doi/10.1126/science.adu8943
Materials and Methods; Supplementary Text; Figs. S1 to S19; Movies S1 to S9
Submitted 26 November 2024; accepted 20 June 2025
10.1126/science.adu8943